Shahid Chamran University of Ahvaz

Iranian Association of Electrical and Electronics Engineers

Journal of Applied Research in Electrical Engineering

E-ISSN: 2783-2864
P-ISSN: 2717-414X
Homepage: https://jaree.scu.ac.ir/

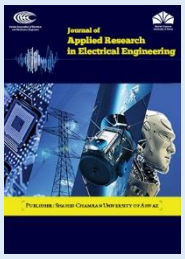

Research Article

Design and Parameter Estimation of Series Resonant Induction Heating Systems Using Self-Oscillating Tuning Loop

Behzad Jaafari, and Alireza Namadmalan *

Department of Electrical and Computer Engineering, Jundi-Shapur University of Technology, Dezful 64615-334, Iran

** Corresponding Author: namadmalan@jsu.ac.ir*

Abstract: This paper presents a design procedure and a new control method for power regulation of series resonant Induction Heating (IH) systems using a self-oscillating tuning loop. The proposed power regulator can accurately estimate the instantaneous phase angle and the main parameters of the resonant load. Moreover, the power control algorithm is devised based on a combination of Phase Shift (PS) and Pulse Density Modulation (PDM) methods. For simplicity, the tuning loop utilizes the PS control method for power regulation. Moreover, the Pulse Density Modulation (PDM) and frequency-sweep methods can be used in the proposed tuning loop. The new method is verified by a laboratory prototype with an output power of about 220 W and an operating frequency of about 60 kHz.

Keywords: Self-Oscillating tuning loops, induction heating systems, phase-shift control, series resonant inverters.

Article history
Received 13 March 2021; Revised 10 April 2021; Accepted 18 April 2021; Published online 30 June 2021.

How to cite this article
B. Jaafari, and A. Namadmalan, "Design and parameter estimation of series resonant induction heating systems using self-oscillating tuning loop," *J. Appl. Res. Electr. Eng.*, vol. 1, no. 1, pp. 42-49, 2022.
DOI: 10.22055/jaree.2021.36904.1025

Check for updates

1. INTRODUCTION

Induction Heating (IH) systems play a fundamental role in modern heating systems such as annealing, hardening, and melting furnaces and cooking systems [1-7]. IH systems commonly require a medium- or high-frequency current or voltage source of power supply with fixed or variable frequencies. The resonant inverters are widely used to supply IH systems because of their near sinusoidal waveforms, less Electromagnetic Interference (EMI), and switching losses [3-5,7-9].

Two common types of resonant inverters are voltage source and current source inverters among which voltage source resonant inverters are commonly used due to their reliability and various controlling methods [2,4,10-12]. Resonant inverters are named after their resonant tank configuration, such as Series Resonant Inverters (SRIs), Parallel Resonant Inverters (PRI), and Series-Parallel Resonant Inverter (SPRI) [2,12,13]. Among the voltage source resonant inverters, SRIs are more common for IH systems as they have various control methods, more stability in frequency tuning, and simplicity in load estimation and regulation [15-19].

For SRIs, there are four common methods for power and frequency regulations, i.e., Frequency-Sweep (FS) [20], Phase-Shift (PS) control [2,21], Pulse Width Modulation (PWM) [12,22,23], and Pulse Density Modulation (PDM) [1,11,24-26]. FS methods require complex algorithms for uncertainties and load variations. Moreover, FS methods have a slow response time for power and frequency tuning. In PS, PWM, and PDM methods, the frequency tuning loop is based on Phase-Locked Loop (PLL) [7,11,27] or Self-Oscillating Switching (SOS) methods [5,10,28]. PLL circuits are sensitive to uncertainties and have stability problems, while SOS circuits have a fast response and are more reliable and uncertainty-tolerant [5].

Recently, SOS techniques have been proposed for power and frequency tuning loops of resonant converters due to their simple circuit and reliability in uncertainties. SOS methods have a quick response in frequency tuning and power regulation. Moreover, by developing SOS tuning loops, PDM, PS, and FS methods can be utilized in one of the switching frequency harmonics [5].

Besides the benefits of SOS methods, previous works have no straightforward design procedure for the tuning loop parameters. The aim of this paper is to present a design

procedure for the desired load variations and operating frequencies.

Moreover, this paper presents a new power regulation method based on the SOS tuning loops, which has a simple structure and estimates the load and its phase angle for an SRI instantly. The proposed control method is based on a combination of a first-order phase-shifter and PDM, which can properly regulate the output power [5].

One of the main problems associated with a well-designed power and frequency tuning loop is its robustness under uncertainties of the resonant tank. Typically, parameters of IH systems have tolerances of about 20%-50%, especially in their working coils. The presented solution can simply estimate the main parameters of the SRI at start-up duration for effective prediction and regulation of the power.

The presented analysis shows that the proposed method properly regulates power for practical deviations and errors in parameters' estimation. The new method estimates the instantaneous phase displacement of the load without phase detector circuits and reduces the time response and robustness of the tuning loop.

The paper is organized as follows. Section 2 presents the modeling of SRIs, the new tuning loop, and the design procedure. Section 3 discusses a power regulation method and parameters' estimation. Sections 4 and 5 present the experimental results and main conclusions of the paper.

2. System Modelling and Design Consideration

A schematic of a half-bridge SRI based on the SOS tuning loop is shown in Fig. 1, while the tuning loop can be applied for a full-bridge SRI. The main units of the tuning loop are a Current Transformer (CT), a lead phase-shifter, a Zero-Detector, a Micro Controller Unit (MCU), and logic gates.

For simplicity, the PS unit is considered a first-order leading phase shifter circuit that can properly make phase displacement, φ, up to $+45^0$. Phase displacement is controlled by changing a tuning resistor, R_T, implemented by a digital potentiometer connected to the MCU. The Zero-Detector unit is constructed by an ultra-fast comparator, LT1016, which improves the performance of the tuning loop at start-up cycles. As seen from Fig. 1, the gate driver of the SRI is based on the bootstrap technique, IR2104S, so the low side switch, S1, must be kept turn on before start-up to ensure the charging of the bootstrap capacitor.

At start-up, the high side switch, S2, is turned on and S1 is turned off, so a step voltage is applied to the series resonant load, and the resonant current, I_o, flows into the load. The start-up begins by enabling the MCU's starting signal, *Sig*, as connected to the AND gate. As is seen from Fig. 1, the phase of the measured current is made lead using the PS block shifts. The zero crossing of the PS unit changes the state of the power switches. At the first zero crossing, the state of the switches is changed and continuously repeats for the next cycles [5].

As described, the output voltage of the SRI, V_o, will be lead with respect to I_o with a phase displacement of φ at steady-state conditions. Hence, the PS block controls the output power by shifting the phase of the SRI. The following sections present the main equations of the SRI and the design procedure of the tuning loop.

2.1. SRI and Formulation

As shown in Fig. 1 and described in the SOS principle of operation, SRI generates square wave output voltage, V_o, with a duty cycle of about 50%. Equations of V_o, output current, I_o,

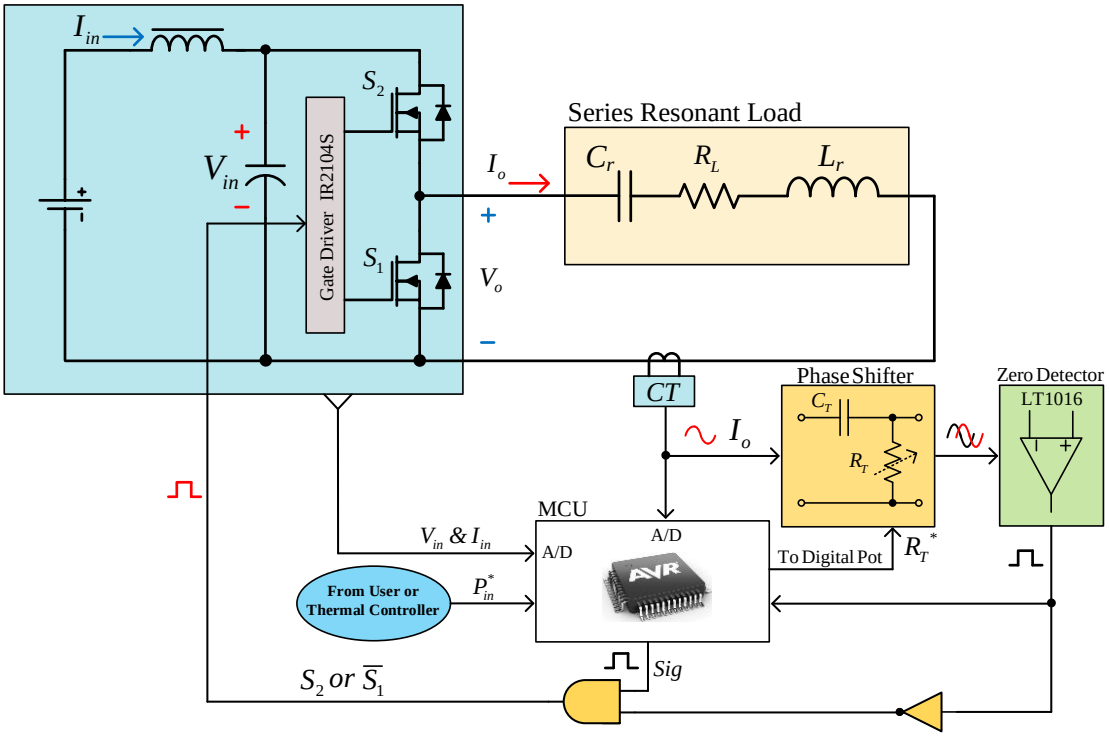

Fig. 1: A schematic of the half-bridge SRI based on the proposed SOS power and frequency tuning loop.

and series resonant impedance, $Z(j\omega_s)$, are given by (1), (2), and (3) as follows considering fundamental harmonic approximation:

$$V_o(t)=\sum_{n=1}^{\infty}\frac{2V_{in}}{n\pi}\sin(n\omega_s t), \quad for\ n=1,3,5,... \tag{1}$$

$$I_o(t)\approx\frac{2V_{in}}{\pi\,|\,Z(j\omega_s)\,|}\sin(\omega_s t-\varphi). \tag{2}$$

$$Z(j\omega_s)=\left(j\omega_s L_r-\frac{j}{\omega_s C_r}+R_L\right). \tag{3}$$

where V_{in} is the dc-link voltage of SRI, $Z(j\omega_s)$ is the load impedance of SRI, ω_s is the angular switching frequency, φ is the phase angle between the output voltage and current, L_r is the equivalent resonant inductance, R_L is the summation of the intrinsic resistance of working coil and reflected load resistance, and C_r is the value of the resonant capacitor. The quality factor, Q, damping factor, ζ, natural frequency, f_n, and the characteristic impedance, Z_0, are derived as follows:

$$Q=\frac{1}{2\zeta}=\frac{Z_0}{R_L}. \tag{4}$$

$$Z_0=\sqrt{\frac{L_r}{C_r}},\ f_n=\frac{1}{2\pi\sqrt{L_r C_r}}. \tag{5}$$

The relation between natural-frequency, f_n, and resonant-frequency, f_r, where Zero Voltage and Zero Current Switching (ZVZCS) occurs, is derived by (6):

$$f_r=\frac{1}{2\pi}\sqrt{\frac{1-\zeta^2}{L_r C_r}}=f_n\sqrt{1-\zeta^2}. \tag{6}$$

Regarding Fig. 1, the lead phase-shifter makes phase displacement equal to φ, which is derived by (7) with respect to its tuning resistor, R_T, and capacitor, C_T:

$$\varphi=\tan^{-1}\left(\frac{1}{\omega_s\tau_T}\right),\quad \tau_T=R_T C_T. \tag{7}$$

The tuning resistor, R_T, can be an adjustable digital potentiometer controlled by an MCU. On the other hand, the phase displacement of the series resonant load can be derived using fundamental harmonic approximation as follows:

$$\angle Z(j\omega_s)=tan^{-1}\left(\frac{\omega_s^2\omega_n^{-2}-1}{\omega_s R_L C_r}\right). \tag{8}$$

Phase displacement of the PS unit is approximately equal to the phase of $Z(j\omega_s)$, so the switching frequency of the SRI can be derived by solving (7) and (8), as derived by (9).

$$\omega_s=\omega_n\sqrt{1+\frac{R_L C_r}{R_T C_T}}. \tag{9}$$

Regarding (9), (7) can be rewritten by (10) as a function of the PS unit parameters:

$$\varphi=\tan^{-1}\left(\frac{1}{\alpha\sqrt{1+\frac{1}{\alpha Q}}}\right),\quad \alpha=\tau_T\omega_n\approx\tau_T\omega_r. \tag{10}$$

where τ_T is the time constant and α is the normalized time constant of the phase-shifter with respect to ω_n. Regarding φ, the output power, P_o, of the SRI can be approximated by (11) as a function of α. To show the accuracy of the above equations, simulations are done based on the PSIM simulator with V_{in} = 70 V, Q = 10, C_r = 250 nF, and L_r = 50 µH. C_T is 2 nF, and R_T is considered variable.

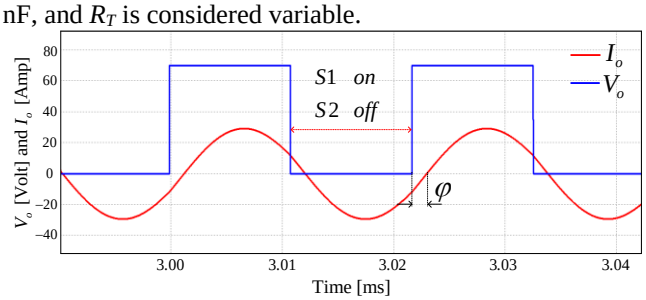

Fig. 2: The output voltage, V_o, and current, I_o, of the SRI at steady-state conditions with $\varphi\approx 21^0$, V_{in} = 70 V, Q = 10, C_r = 250 nF, L_r = 50 µH and an operating frequency of about 45.95 kHz.

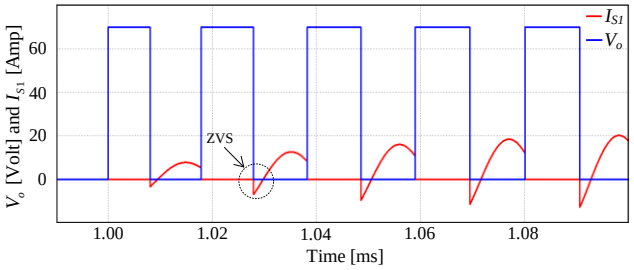

Fig. 3: The output voltage of SRI, V_o, and current of S1, I_{S1}, at start-up conditions using the SOS method with Q = 10, R_T = 2 kΩ, and V_{in}=70 V.

Regarding the mentioned parameters, natural frequency and resonant frequency are about 45.016 kHz and 44.960 kHz, respectively. Fig. 2 shows I_o and V_o at steady-state conditions with $\alpha\approx 2.262$, i.e., R_T = 4 kΩ. Regarding Fig. 2, f_s and φ are about 45.95 kHz and 21^0 while considering (9), f_s is derived to be 45.93 kHz. Fig. 3 shows the current of S1, I_{S1}, and V_o at start-up while Zero Voltage Switching (ZVS) is achieved at the beginning cycles.

$$P_o\approx\frac{1}{2}\left(\frac{2V_{in}}{\pi\,|\,Z(j\omega_s)\,|}\right)^2 R_L=\frac{2(V_{in}\cos\varphi)^2}{\pi^2 R_L},$$

$$P_o(\alpha)=\frac{2V_{in}^{\ 2}}{\pi^2 R_L}\cos^2\left(\tan^{-1}\left(\frac{1}{\alpha\sqrt{1+\frac{1}{\alpha Q}}}\right)\right). \tag{11}$$

One of the most important advantages of the SOS methods is their ability to predict parameters of SRI load. Regarding Fig. 3, the natural frequency of the SRI can be predicted at the beginning cycles of the start-up by counting intervals between zero crossings of the ZD unit directly connected to the MCU, as is seen in Fig. 1. To accurately detect f_r, it is proposed to start and stop SRI for a few cycles in minimum phase displacement, φ_{min}. For an SRI utilized for IH systems, quality factors are larger than 5, so $f_n\approx f_r$ and L_r can be derived by detecting f_r for a known resonant capacitor and using (5).

2.2. Design Procedure

The main parameters for the design of an SRI based on the SOS tuning loop are calculating V_{in}, the variation range of RT, and tuning capacitor according to the resonant load parameters. Considering the maximum output power, P_o^{max}, which occurs at the minimum phase angle, $\varphi_{min} \approx 10^0$, the required dc-link voltage is designed by (13) for the maximum value of the equivalent load resistance, R_L^{max}. The minimum phase displacement is considered to ZVS operation SRI.

$$V_{in} = \sqrt{\frac{\pi^2 P_o^{\max} R_L^{\max}}{2\cos^2 \varphi_{\min}}}. \tag{13}$$

The range of the tuning resistor, R_T, must be determined for the PS unit. Regarding (10) and considering φ_{min} and Q_{min}, as well as the minimum value of the normalized time constant of the PS, α_{min} can be calculated by solving (14), which has two answers, but the acceptable one is positive and is derived by (15). Hence, assuming C_T and the possible minimum natural angular frequency, ω_n^{min}, the upper limit of R_T can be obtained by (16):

$$\alpha_{\max}^2 + Q_{\min}^{-1}\alpha_{\max} - \left(\tan\varphi_{\min}\right)^{-2} = 0. \tag{14}$$

$$\rightarrow \alpha_{\max} = \frac{\sqrt{1+\left[2Q_{\min}\left(\tan\varphi_{\min}\right)^{-1}\right]^2}-1}{2Q_{\min}}. \tag{15}$$

$$\rightarrow R_{T,\max} = \frac{\alpha_{\max}}{\omega_n^{\min} C_T}. \tag{16}$$

To obtain the lower limit of the tuning resistor, R_T, it is necessary to determine φ_{max}, according to P_o^{min}. The maximum amount of the possible phase displacement in the first-order phase-shifter is 45^0, which reduces the output power to about 50%. Hence, by using (11) and determining P_o^{min}, the maximum phase of the PS is calculated from (17). Thus, by having φ_{max}, the minimum normalized time constant of the phase-shifter can be obtained using (18), i.e., similar to (15). Regarding (18), the minimum normalized time constant is derived at the possible maximum natural angular frequency, ω_n^{max}, of the system.

$$\alpha_{\min} = \frac{\sqrt{1+\left[2Q_{\max}\left(\tan\varphi_{\max}\right)^{-1}\right]^2}-1}{2Q_{\max}}. \tag{17}$$

$$\rightarrow R_T^{\min} = \frac{\alpha_{\min}}{\omega_n^{\max} C_T}. \tag{18}$$

3. Power Control and Parameters' Estimation

For simplicity in analyses, the first-order PS is analyzed in the above formulations, which can properly regulate the output power up to 50%. For wider power regulation, power, the PS technique, and PDM are used simultaneously.

As shown in Fig. 1, in this paper, the input current and voltage are measured to calculate instant input power, P_{in}. Since the losses of the half-bridge inverter and dc-link filter are typically less than 5%, so the input power is measured and regulated instead of the output power of the inverter for simplicity. Using (7) and the measured switching frequency, MCU calculates the instantaneous phase displacement, φ. Regarding Fig. 1, P_{in}^* is considered the reference input power, which can be applied from the user or output of a thermal controller. In the proposed control method, the reference phase displacement, φ^*, can be calculated using (11) with respect to φ and the ratio P_{in}^* and P_{in}, as derived by (19).

$$\varphi^* = \cos^{-1}\left(\cos\varphi \times \sqrt{\frac{P_{in}^*}{P_{in}}}\right). \tag{19}$$

For IH systems, the quality factor is typically larger than 5 or $\zeta < 0.1$. Therefore, the resonant frequency is equal to the natural frequency with good approximation, i.e., $f_n \approx f_r$. Moreover, the quality factor is not changed much for designing a specific load.

In practice, due to the uncertainties of the resonant tank like the aging effect in the resonant capacitor or variations in the resonant tank parameters during the heating treatments, the estimations are prone to errors and deviations.

One of the main problems associated with a well-designed power and frequency tuning loop is its robustness under uncertainties of the load variations.

Practically, the input power and Po can be considered approximately equal to calculate equivalent series resistance, R_L. Moreover, at steady-state conditions, the phase displacement can be calculated by (7) using τ_T and detecting the instant switching frequency, f_s. As a result, R_L can be estimated using the following equation:

$$P_o \approx P_{in} = V_{in} I_{in}, \quad \rightarrow R_L \approx \frac{2(\cos\varphi)^2 V_{in}}{\pi^2 I_{in}}. \tag{20}$$

Regarding trigonometric rules and (7), R_L can be rewritten as follows:

$$\cos^2\varphi = \frac{\left(\omega_s\tau_T\right)^2}{1+\left(\omega_s\tau_T\right)^2}. \tag{21}$$

$$R_L \approx \frac{2V_{in}}{\pi^2 I_{in}}\left(\frac{\left(\omega_s\tau_T\right)^2}{1+\left(\omega_s\tau_T\right)^2}\right). \tag{22}$$

Moreover, the PDM is used simultaneously when the reference phase displacement is greater than 45° from (19). Hence, the R_L should be estimated using (23) for wider power regulation.

$$R_L \approx \frac{2V_{in}D}{\pi^2 I_{in}}\left(\frac{\left(\omega_s\tau_T\right)^2}{1+\left(\omega_s\tau_T\right)^2}\right), \quad D = \frac{T_{on}}{T_{on}+T_{off}}. \tag{23}$$

where D is the duty cycle of the MCU's squared signal, Sig, and T_{on} and T_{off} are the time duration in which the Sig turns on and off, respectively. Furthermore, at steady-state conditions, the summation of T_{on} and T_{off} should be much larger than the time period of the output current.

To apply the PDM technique, it is necessary to calculate the reference duty-cycle, D^*. Therefore, the reference duty-cycle can be obtained from (24):

$$D^* = \frac{2\pi^2 R_L P_{in}^*}{V_{in}^2 Cos^2 \varphi^*} = \frac{\pi^2 R_L P_{in}^*}{V_{in}^2}. \quad (24)$$

where φ^* is set to 45°.

Like (15) and (17), the reference tuning resistor, R_T^*, can be calculated using (25) as follows:

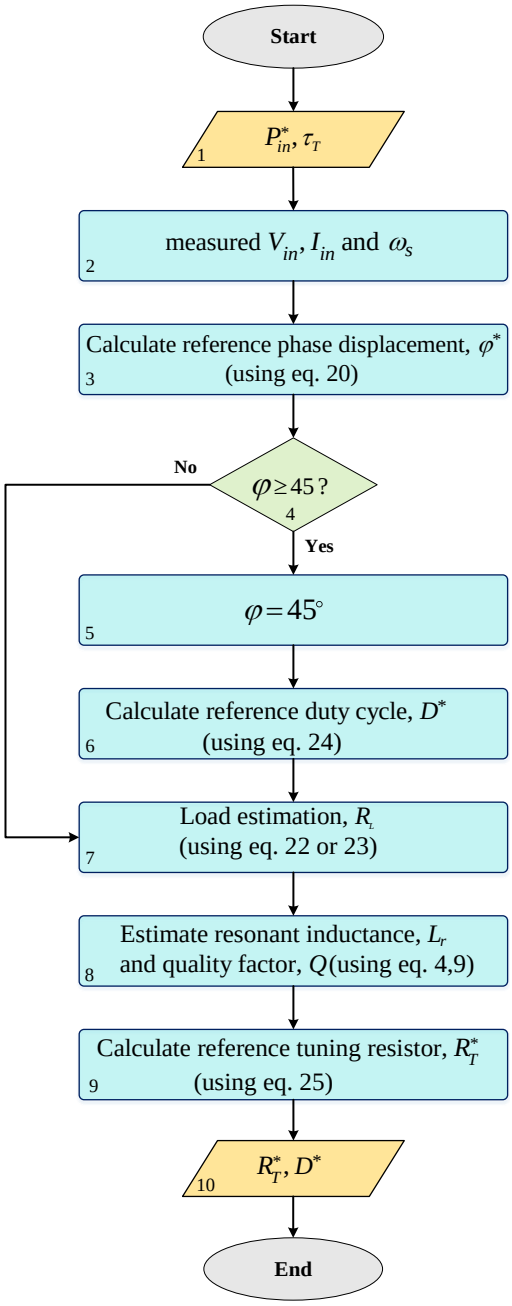

Fig. 4: The flowchart of the power regulation

$$\alpha^* = \frac{\sqrt{1+\left[2Q\left(\tan\varphi^*\right)^{-1}\right]^2}-1}{2Q}, \quad (25)$$

$$\rightarrow R_T^* = \frac{\alpha^*}{\omega_n C_T}.$$

Fig. 4 illustrates the flowchart of the proposed power regulation procedure and the parameters' estimation of tuning loops. In the proposed method, the MCU receives P_{in}^*, C_r, and τ_T as inputs. In practice, C_r and C_T are fixed values and could be estimated using their step responses. To estimate output power, the input voltage and current are measured. The switching-frequency can estimate instantly. Moreover, the MCU can estimate natural-frequency in initial cycles when the phase displacement is considered minimum. Using (22), R_L can estimate when the PS technique is used alone. When the PS technique and PDM are used simultaneously, RL should be estimated using (23).

Moreover, the value of L_r can be estimated by (4), (9), τ_T, and C_r. Therefore, regarding (10) and C_T, the value of the reference tuning resistor, R_T^*, is determined. Then, R_T^* is applied to the PS unit. Hence, the input power can instantly track the reference input power with fewer transients, which reduces the possible voltage and current stresses of the SRI.

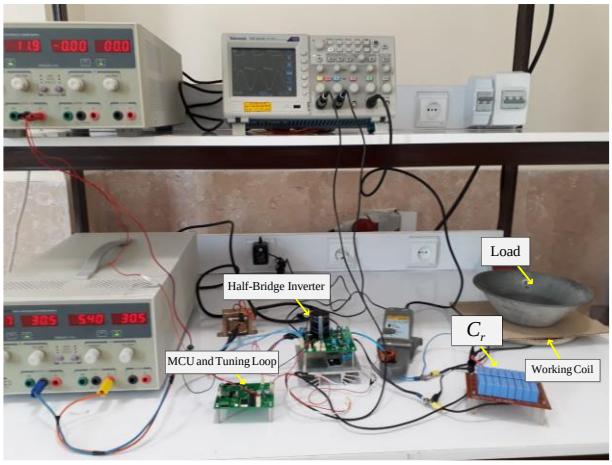

Fig. 5: The experimental setup of the IH system based on the SOS method.

Hence, for an instant quality factor, the measured P_{in} and the estimated L_r and ω_s, instant φ, and the reference parameters can be calculated with negligible errors according to the reference input power, i.e., (24) and (25).

As was already described, the presented control method can simply estimate the main parameters of the SRI at start-up duration for effective prediction and regulation of the power. Basically, the behavior of the proposed power regulating loop directly depends on the estimation of φ.

4. Experimental Results

A laboratory prototype was developed based on the designing method proposed in Section 2. Fig. 5 shows an experimental setup of the IH system based on the SOS power and frequency tuning loop. The parameters of the half-bridge inverter and the tuning system are given in Table 1. The half-bridge inverter is constructed by two IRFP250 power MOSFETs, S1 and S2, and IR2104 gate driver. SRI is designed for a maximum input voltage of 100 V. The tuning loops are constructed by logic elements, ATMEGA8 MCU, and LT1016 comparator for zero detector units.

The value of the load, R_L, is about 1.92 Ω, which is estimated at the steady-state operation using (22). According to (4), the characteristic impedance, Z_r, is estimated at 12.14 Ω while the natural-frequency, f_r, and the value of C_r are 52.44 kHz and 250 nF, respectively. Hence, the quality factor is about 6.3 using (4). For the working coil, a spiral coil with an inner diameter of 5 cm and outer diameters of 20 cm is used. The spiral coil is wound with a Litz wire that is built

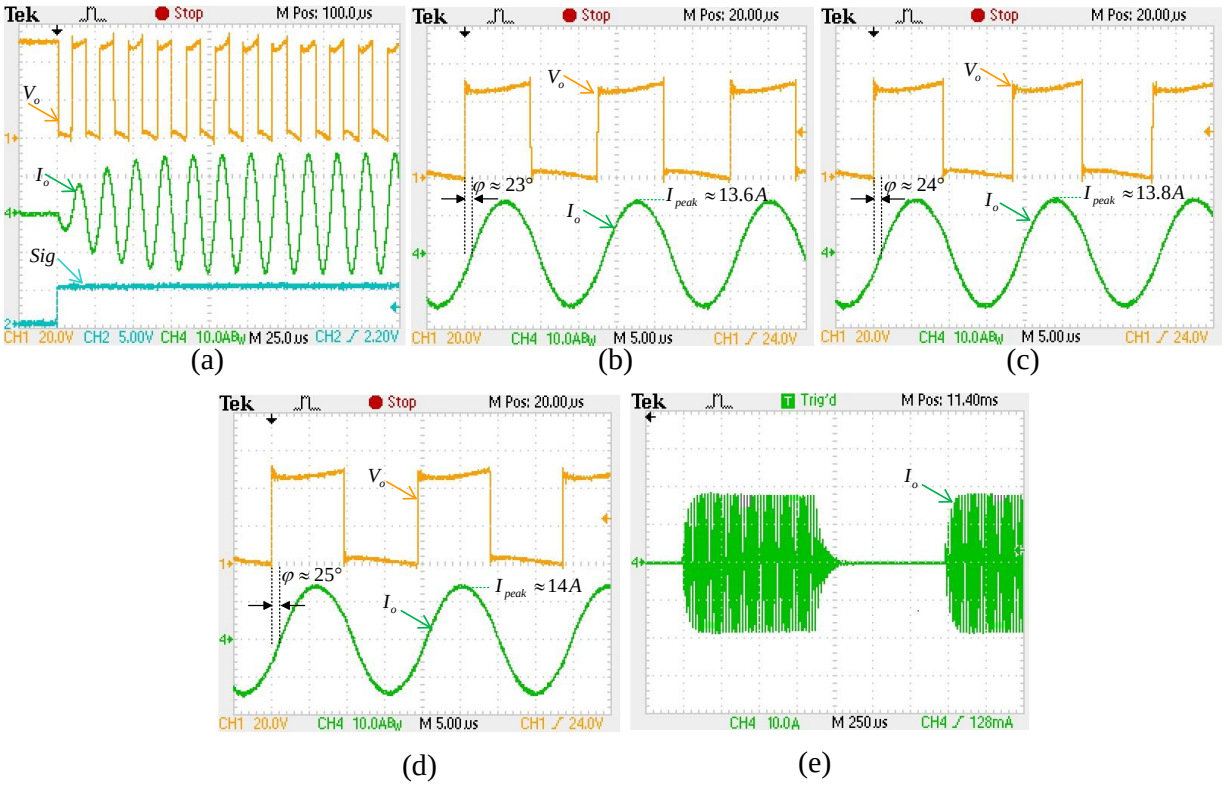

Fig. 6: (a) *Sig*, V_o and I_o at start-up conditions with $Q \approx 6.3$, $C_r \approx 250$ nF, $V_{in} \approx 50$ V. (b) V_o and I_o at 10% decrease in the capacitor and steady-state conditions with $f_s \approx 56$ kHz, $\alpha \approx 2$, $C_r \approx 225$ nF, $V_{in} \approx 50$ V. (c) V_o and I_o without deviation in C_r while $f_s \approx 54$ kHz, $\alpha \approx 2$, $C_r \approx 250$ nF, $V_{in} \approx 50$ V. (d) V_o and I_o for 10% increase in C_r while $f_s \approx 56$ kHz, $\alpha \approx 2$, $C_r \approx 275$ nF, $V_{in} \approx 50$ V. (e) I_o in the PDM technique for the SOS method with $D \approx 50\%$ while frequency of *Sig* is about 580 Hz.

with 19 insulated strands Lacquered wire. For 19 turns and loading effect from the pot, L_r is about 36.84 µH, and the material of the pot is iron. The air gap between the pot and coil is considered 5 mm. Fig. 6(a) shows the input signal, Sig, the output voltage, the current, V_o, and I_o, of the IH system at the start-up conditions. Regarding Fig. 6(a), the IH system based on SOS has a proper dynamic in transient conditions.

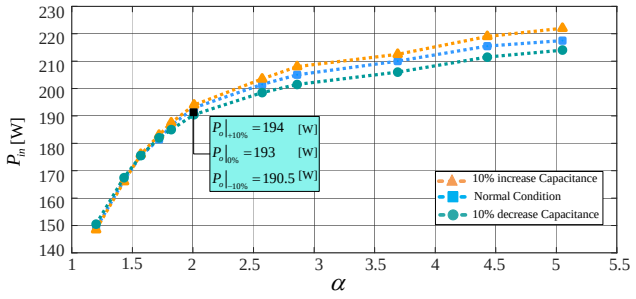

Fig. 7: Input power curve, P_{in}, in different normalized time constants in which the sweeping phase shifts approximately from 10° to 42°.

In order to analyze the sensitivity of the proposed method, three practical steps are performed. The first step is to reduce the capacitor by 10% ($C_r \approx 225$ nF) and record the input power and the tuning resistance, R_T, or record the normalized time constant of the phase shifter, α.

At steady-state, for input power, Pin, of about 190.5 W, the normalized time constant and phase displacement are about 23°, which are shown in Fig. 6(b). The second step is to test under normal conditions, i.e., $C_r \approx 250$ nF, while P_{in} is about 193 W for $\alpha \approx 2$ and $\varphi \approx 24^{\circ}$ as shown in Fig. 6(c). Regarding simulations and formulations, the output power is calculated to be about 189 W. In the last step, the capacitor increases by 10%, i.e., $C_r \approx 275$ nF. Fig. 6(d) shows the output voltage and current in these conditions while Pin is measured to be 194 W for $\alpha \approx 2$ and $\varphi \approx 25°$. Fig. 6(e) displays the output current of the IH system when the PDM technique is used for the SOS method with $D \approx 50\%$ and signal-frequency of about 580 Hz.

Table 1: The design information of the IH system and tuning loop for the laboratory prototype

Parameter	Quantity
Input voltage, V_{dc}	50 [V]
Maximum input power, P_{in}	220 [W]
Minimum phase delay	10 [degrees]
R_T	10 kΩ potentiometer
C_T	2 [nF]
Q	~6.3
C_r	250 [nF]
L_r (with pot)	38.6 µH
Comparator for ZD unit	LT1016
Power MOSFETs	IRFP250
Gate driver	IR2104
Logic element	74HC04, 74HC08
Opto-couplers	6N137

Finally, the input power of the SRI is measured for different values of α and the variations in the resonant capacitor as shown in Fig. 7. Regarding Fig. 7, there are larger power deviations for the higher values of α in comparison with the lower values of α. This phenomenon relates to the SRI and dc-link filter losses and variations in equivalent

resistance caused by the deviation of the resonant frequency. However, the deviations can be neglected.

In general, there are two kinds of changes in the load, either due to the type of work-piece material, such as steel, aluminum, etc. or due to the frequency variations. In this IH system, the load changes only by changing the frequency.

According to Fig. 7, in $\alpha \approx 5$ or $\varphi \approx 10°$ and for 10% increase, the maximum power difference is about 2%. This difference is very low and results from changing the load caused by a change in the resonant frequency. Hence, this is an advantage in large phases, i.e., $\alpha < 2$, while these deviations almost neutralize each other and make the total power deviation to be less than 0.5%, as seen from Fig. 7. Therefore, the practical estimation deviations and errors are very low, and the tuning loops can adjust the power more accurately.

5. Conclusions

This paper presents a design procedure and a new power regulation algorithm for series resonant IH systems based on a tunable self-oscillating tuning loop. The proposed method accurately estimates instant phase displacement, resonant frequency, equivalent load resistance, and inductance of the SRI. Based on the estimations, the instant power reference can be tuned with low transients, which is important for high-power IH systems. To show the accuracy of the proposed method, experimental tests have been done for possible estimation deviations. Experimental results show that using the proposed power tuning loop, negligible power deviations occur, about 2%, under large tolerances in the resonant tank circuit.

CRediT Authorship Contribution Statement

Behzad Jaafari: Data curation, Formal analysis, Investigation, Software. **Alireza Namadmalan:** Conceptualization, Investigation, Project administration, Supervision, Validation, Roles/Writing - original draft, Writing - review & editing.

Declaration of Competing Interest

The authors declare that they have no known competing financial interests or personal relationships that could have appeared to influence the work reported in this paper. The ethical issues; including plagiarism, informed consent, misconduct, data fabrication and/or falsification, double publication and/or submission, redundancy has been completely observed by the authors.

References

[1] VB. Devara, V. Neti, T. Maity, et al., "Capacitor-sharing two-output series-resonant inverter for induction cooking application", *IET Power Electronics*, Vol. 9, no. 11, pp. 2240-2248, 2016.

[2] V. Esteve, J. Jordán, E. Sanchis-Kilders, et al., "Improving the reliability of series resonant inverters for induction heating applications", *IEEE transactions on industrial electronics*, Vol. 61, no. 5, pp. 2564-2572, 2014.

[3] O. Lucia, J. Acero, C. Carretero, et al., "Induction heating appliances: Toward *more* flexible cooking surfaces", *IEEE Industrial Electronics Magazine*, Vol. 7, no. 3, pp. 35-47, 2013.

[4] O. Lucia, P. Maussion, E.J. Dede, et al., "Induction heating technology and its applications: past developments, current technology, and future challenges", *IEEE Transactions on Industrial Electronics*, Vol. 61 no. 5, pp. 2509-2520, 2014.

[5] A. Namadmalan, "Universal tuning system for series-resonant induction heating applications", *IEEE Transactions on Industrial Electronics*, Vol. 64, no. 4, pp. 2801-2808, 2017.

[6] H. Sarnago, O. Lucia, A. Mediano, et al., "Modulation scheme for improved operation of an RB-IGBT-based resonant inverter applied to domestic induction heating", *IEEE Transactions on Industrial Electronics*, Vol. 60, no. 5, pp. 2066-2073, 2013.

[7] J. Zerad, S. Riachy, P. Toussaint, et al., "Novel Phasor Transformation for Feedback Control Design of Induction Heating Systems With Experimental Results", *IEEE Transactions on Industrial Electronics*, 2015, 62, (10), pp. 6478-6485.

[8] A.R. Namadmalan, S.H. Fathi, J.S. Moghani, et al., "Power quality improvement for three phase current source induction heating systems", in *2011 6th IEEE Conference on Industrial Electronics and Applications* pp. 2580-2584, 2011.

[9] H. Sarnago, O. Lucia, A. Mediano, et al., "Analytical model of the half-bridge series resonant inverter for improved power conversion efficiency and performance", *IEEE Transactions on Power Electronics*, Vol. 30, no. 8, pp. 4128-4143, 2015.

[10] A. Namadmalan, J.S. Moghani, " Single-phase current source induction heater with improved efficiency and package size", *Journal of Power Electronics*, Vol. 13, no. 2, pp. 322-328, 2013.

[11] B. Nagarajan, R.R. Sathi, "Phase locked loop based pulse density modulation scheme for the power control of induction heating applications", *Journal of Power Electronics*, Vol. 15, no. 1, pp. 65-77, 2015.

[12] T. Mishima, S. Sakamoto, C. Ide, "ZVS phase-shift PWM-controlled single-stage boost full-bridge AC–AC converter for high-frequency induction heating applications", *IEEE Transactions on Industrial Electronics*, Vol. 64, no. 3, pp. 2054-2061, 2017.

[13] M. Uno, A. Kukita, "Double-switch equalizer using parallel-or series-parallel-resonant inverter and voltage multiplier for series-connected supercapacitors", *IEEE Transactions on Power Electronics*, Vol. 29, no. 2, pp 812-828, 2014.

[14] A. Namadmalan, "Bidirectional current-fed resonant inverter for contactless energy transfer systems", *IEEE Transactions on Industrial Electronics*, Vol. 62, no. 1, pp. 238-245, 2015.

[15] H.P. Park, J.H. Jung, "Load Adaptive Modulation of Series Resonant Inverter for All-Metal Induction

Heating Applications", *IEEE Transactions on Industrial Electronics*, Vol. 65, no. 9, pp. 6983-6993, 2018.

[16] O. Lucia, J.M. Burdio, I. Millan, et al., "Load-adaptive control algorithm of half-bridge series resonant inverter for domestic induction heating", *IEEE transactions on industrial electronics*, Vol. 56, no. 8, pp. 3106-3116, 2009.

[17] I. Millan, J.M. Burdío, J. Acero, et al., "Series resonant inverter with selective harmonic operation applied to all-metal domestic induction heating", *IET power electronics*, Vol. 4, no. 5, pp. 587-592, 2011.

[18] B.A. Nguyen, Q.D. Phan, D.M. Nguyen, et al., "Parameter Identification Method for a Three-Phase Induction Heating System", *IEEE Transactions on Industry Applications*, Vol. 51, no. 6, pp. 4853-4860, 2015.

[19] N. Domingo, L.A. Barragán, J.M.M. Montiel, et al., "Fast power–frequency function estimation for induction heating appliances", *Electronics Letters*, Vol. 53, no. 7, pp. 498-500, 2017.

[20] L.A. Barragán, D. Navarro, J. Acero, et al., "FPGA implementation of a switching frequency modulation circuit for EMI reduction in resonant inverters for induction heating appliances", *IEEE Transactions on ndustrial Electronics*, Vol. 55, no. 1, pp. 11-20, 2008.

[21] S. Komeda, H. Fujita, "A Phase-Shift-Controlled Direct AC-to-AC Converter for Induction Heaters", *IEEE Transactions on Power Electronics*, Vol. 33, no. 5, pp. 4115-4124, 2018.

[22] T. Mishima, Y. Nakagawa, M. Nakaoka, "A bridgeless BHB ZVS-PWM AC–AC converter for high-frequency induction heating applications", *IEEE Transactions on Industry Applications*, Vol. 51, no. 4, pp. 3304-3315, 2015.

[23] B. Saha, R.Y. Kim, "High power density series resonant inverter using an auxiliary switched capacitor cell for induction heating applications", *IEEE Transactions on Power Electronics*, Vol. 29, no. 4, pp. 1909-1918, 2014.

[24] N.A. Ahmed, "High-frequency soft-switching ac conversion circuit with dual-mode PWM/PDM control strategy for high-power IH applications", *IEEE transactions on industrial electronics*, Vol. 58, no. 4, pp. 1440-1448, 2011.

[25] V.Esteve, J. Jordán, E. Sanchis-Kilders, et al., "Enhanced pulse-density-modulated power control for high-frequency induction heating inverters", *IEEE Transactions on Industrial Electronics*, Vol. 62, no. 11, pp. 6905-6914, 2015.

[26] O. Lucia, H. Sarnago, J. M. Burdio, "Pulse density modulated control for the series resonant multi-inverter for induction heating applications", in *IECON 2016-42nd Annual Conference of the IEEE Industrial Electronics Society*, pp. 5995-6000, 2016.

[27] Gati, E., Kampitsis, G. and Manias, S., "Variable frequency controller for inductive power transfer in dynamic conditions", *IEEE Transactions on Power Electronics*, Vol. 32, no. 2, pp. 1684-1696, 2017.

[28] A. Namadmalan, "Self-oscillating tuning loops for series resonant inductive power transfer systems", *IEEE Transactions on Power Electronics*, Vol. 31, no. 10, pp. 7320-7327, 2016.

BIOGRAPHY

Behzad Jaafari was born in Andimeshk City, Khuzestan, Iran in 1993. He received his B.Sc. degree from the Jundi-Shapur University of Technology (JSU), Dezful, Iran in 2016 and his M.Sc. degree (with hons.) in electrical engineering from the same university in 2018. His current research interests include power electronics, electric vehicles, induction systems, and inductive power transfer.

Alireza Namadmalan received his B.Sc. degree from the Isfahan University of Technology, Isfahan, Iran in 2009 and his M.Sc. and Ph.D. degrees (with hons.) in electrical engineering from the Amirkabir University of Technology, Tehran, Iran in 2011 and 2014, respectively. From 2012 to 2014, he had research activities with the R&D Centre of Damavand Induction Furnace Company, Damavand, Iran where he was working on industrial induction heating systems. He is currently an assistant professor at the Department of Electrical and Computer Engineering, the Jundi-Shapur University of Technology, Dezful, Iran. His current research interests include power electronics, electromagnetic design using finite element methods, inductive power transfer, and renewable energy conversion.